

The IMF from Low to High Redshift

Laura Greggio and Alvio Renzini *

INAF-Osservatorio Astronomico di Padova

Vicolo dell'Osservatorio 5, I-35122, Padova, Italy

Abstract

From time to time, and quite more frequently in recent years, claims appear favoring a variable Initial Mass Function (IMF), one way or another, either in time or space. In this chapter we add our two pennies of wisdom, illustrating how the IMF affects various properties of galaxies and galaxy clusters. We start by showing that even relatively small variations of the IMF slope have large effects on the demography of stellar populations, moving the bulk of the stellar mass from one end to the other of the distribution. We then point out how the slope of the IMF in different mass ranges controls specific major properties of galaxies and clusters. The slope of the IMF below $\sim 1 M_{\odot}$ controls the M/L ratio of local ellipticals, whereas the slope between ~ 1 and $\sim 1.4 M_{\odot}$ controls the evolution with redshift of such ratio, hence of the fundamental plane of elliptical galaxies. Similarly, the slope between ~ 1 and $\sim 40 M_{\odot}$ drives the ratio of the global metal mass in clusters of galaxies to their total luminosity. While we believe that it is perfectly legitimate to entertain the notion that the IMF may not be universal, our message is that when proposing IMF variations to ease a specific problem then one should not neglect to explore the full consequences of the invoked variations.

This paper is integrally reproduced from Chapter 8 of the book by L. Greggio & A. Renzini: *Stellar Populations. A User Guide from Low to High Redshift* (2011, Wiley-VHC Verlag-GmbH & Co., ISBN 9783527409181), whose index is also appended.

*e-mail: laura.greggio@oapd.inaf.it, alvio.renzini@oapd.inaf.it

8

The IMF from Low to High Redshift

At all redshifts much of galaxy properties depend on the IMF, including mass-to-light ratios, derived galaxy masses and star formation rates, the rate of the luminosity evolution of the constituent stellar populations, the metal enrichment, and so on . With so many important issues at stake, we still debate as to whether the IMF is universal, that is, the same in all places and at all cosmic times, or whether it depends on local conditions such as the intensity of star formation (starburst vs. steady star formation), or on cosmic time, for example, via the temperature of the microwave background. As is well known, we do not have anything close to a widely accepted theory of the IMF, and this situation is likely to last much longer than desirable. Again, star formation is an extremely complex (magneto)hydrodynamical process, indeed much more complex than stellar convection or red giant mass loss, for which we already noted the absence of significant theoretical progress over the last 40-50 years. Thus, the IMF is parametrized for example., as one or more power laws or as a log-normal distribution, and the parameters are fixed from pertinent observational constraints. Wherever the IMF has been measured from statistically significant stellar counts, a *Salpeter* IMF has been found, that is, $\phi(M) \propto M^{-s}$, with $s = 1 + x \simeq 2.35$, however with a flattening to $s \simeq 1.3$ below $\sim 0.5 M_{\odot}$. Specifically, where possible, this has been proved for stellar samples including the solar vicinity, open and globular clusters in the Galaxy and in the Magellanic Clouds, actively starbursting regions, as well as the old galactic bulge. Nevertheless, this does not prove the universality of the IMF, as –with one exception– more extreme environments have not been tested yet in the same direct fashion. The exception is represented by the very center the of the Milky Way, in the vicinity of the supermassive black hole, a very extreme environment indeed, where very massive stars seem to dominate the mass distribution. In this chapter we discuss a few aspects of the IMF, using some of the stellar population tools that have been illustrated in the previous chapters, and exploring how specific integral properties of stellar populations depend on the IMF slope in specific mass intervals. In particular, the dependence on the IMF of the mass-to-light ratio of stellar populations is illustrated, along with its evolution as stellar populations passively age. Then the M/L ratios of synthetic stellar populations, and their time evolution, are compared to the dynamical M/L ratios of local elliptical galaxies, as well as to that of ellipticals up to redshift ~ 1 and beyond.

These comparisons allow us to set some constraint on the low-mass portion of the IMF, from ~ 0.1 to $\sim 1.4 M_{\odot}$. A strong constraint of the IMF slope from $\sim 1 M_{\odot}$ up to $\sim 40 M_{\odot}$ and above is then derived from considering the metal content of clusters of galaxies together with their integrated optical luminosity.

8.1 How the IMF Affects Stellar Demography

For a fixed amount of gas turned into stars, different IMFs obviously imply different proportions of low mass and high mass stars. This is illustrated in Figure 8.1 showing three different IMFs, all with the same slope below $0.5 M_{\odot}$, that is $s = 1 + x = 1.35$, and three different slopes above:

$$\begin{aligned} \phi(M) &= A M^{-s} && \text{for } M \geq 0.5 M_{\odot} \\ &= 0.5^{1.3-s} A M^{-1.3} && \text{for } M \leq 0.5 M_{\odot} \end{aligned} \quad (8.1)$$

where the factor $0.5^{1.3-s}$ ensures the continuity of the IMF at $M = 0.5 M_{\odot}$. The normalization of the three IMFs corresponds to a fixed amount \mathcal{M} of gas turned into stars, that is, for fixed

$$\mathcal{M} = \int_{0.1}^{120} M \phi(M) dM. \quad (8.2)$$

Here the case $s = 2.35$ corresponds to the Salpeter-diet IMF already encountered in previous chapters. Thick lines in Figure 8.1b show the cumulative

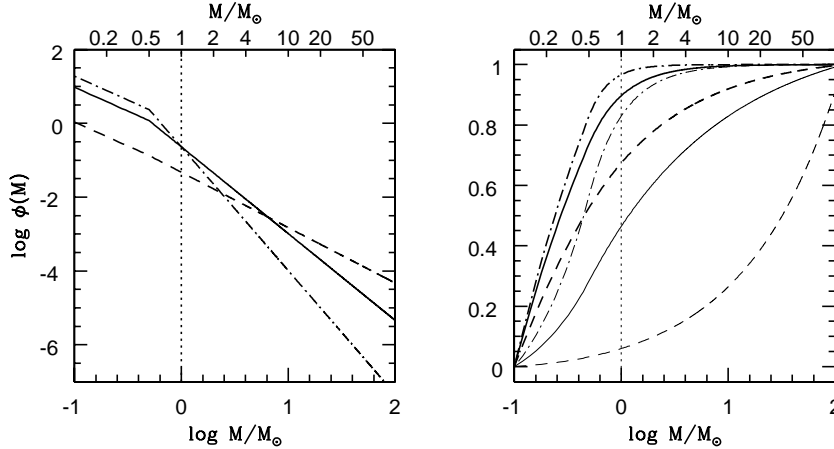


Figure 8.1: Left: three different IMFs normalized to have the same total stellar mass of $1 M_{\odot}$. Below $0.5 M_{\odot}$ all three IMFs have the same slope $s = 1.3$ and above it $s = 1.5$, 2.35 (Salpeter) and 3.35 , shown as dashed, solid, and dot-dashed lines, respectively. Right: cumulative distributions of the number (thick lines) and of the stellar mass (thin lines) for the three IMFs with the same line encoding as in the left panel.

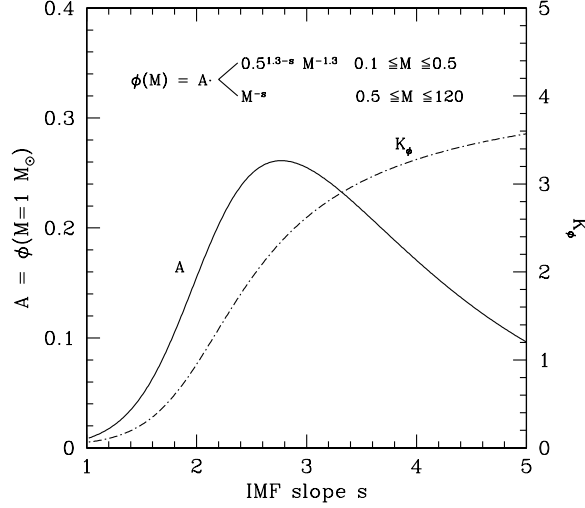


Figure 8.2: The scale factor A as a function of the IMF slope. All IMFs are normalized to a unitary total mass. Also shown is the corresponding mass-to-number conversion factor K_ϕ , such that the total number of stars is given by K_ϕ times the mass turned into stars (in solar units).

distributions, defined as the number of stars with mass less than M , $N(M' < M) = \int_{0.1}^M \phi(M') dM'$, while thin lines show the fraction of mass in stars less massive than M . In a Salpeter-diet IMF $\sim 0.6\%$ of all stars are more massive than $8 M_\odot$, while for $s = 3.35$ and 1.5 these fractions are 0.03% and 9% respectively. The mass in stars heavier than $8 M_\odot$ is 20% for a Salpeter-diet IMF; it drops to 1% for $s = 3.35$, and is boosted to 77% for $s = 1.5$, a *top-heavy* IMF. Figure 8.1 wants to convey the message that IMF variations have a drastic effect on stellar demography, and therefore on several key properties of stellar populations. Suffice it to say that most of the nucleosynthesis comes from $M > 10 M_\odot$ stars, whereas the light of an old population (say, $t > 10$ Gyr) comes from stars with $M \simeq 1 M_\odot$, and therefore is proportional to $\phi(M = M_\odot)$.

Figure 8.2 shows the variation of scale factor A (cf. Chapter 2) as a function of the IMF slope, again for a fixed amount \mathcal{M} of gas turned into stars. The scale factor A has a maximum for $s \simeq 2.75$, pretty close to the Salpeter's slope. Since by construction $A = \phi(M = 1 M_\odot)$ and the luminosity of a $\gtrsim 10$ Gyr old population is proportional to $\phi(M = 1 M_\odot)$, an IMF with the Salpeter's slope has the remarkable property of almost maximizing the light output of an old population, for fixed mass turned into stars. A flat IMF ($s = 1.35$) is much less efficient in this respect, indeed by a factor of ~ 8 compared to the Salpeter's slope, as shown by Figure 8.2. This figure also shows the mass-to-number conversion factor K_ϕ , giving the number of stars N_T formed out of a unit amount of gas turned into stars, that is, $N_T = K_\phi \mathcal{M} / M_\odot$. Thus, for a Salpeter-diet IMF $K_\phi \simeq 1.5$, saying that ~ 150 stars are formed out of $100 M_\odot$

of gas turned into stars.

An empirically motivated, broken-line IMF such as that shown in Figure 8.1 is widely adopted in current astrophysical applications, yet Nature is unlikely to make such a cuspy IMF. Perhaps a more elegant rendition of basically the same empirical data is represented by a Salpeter+lognormal distribution in which a lognormal IMF at low masses joins smoothly to a Salpeter IMF at higher masses, that is:

$$M\phi(M) = \begin{cases} A_1 \exp[-(\text{Log } M - \text{Log } M_c)^2/2\sigma^2], & \text{for } M \leq 1 M_\odot \\ A_2 M^{-x}, & \text{for } M > 1 M_\odot \end{cases} \quad (8.3)$$

where $A_1 = 0.159$, $M_c = 0.079$, $\sigma = 0.69$, $A_2 = 0.0443$ and $x = 1.3$. Thus, this *Chabrier* IMF is almost identical to the Salpeter IMF above $1 M_\odot$, and smoothly flattens below, being almost indistinguishable from the Salpeter-diet IMF.

Explorations of variable IMFs can be made by either changing its slope, or by moving to higher/lower masses the break of the IMF slope with respect to Equation (8.1), or allowing the characteristic mass M_c in Equation (8.3) to vary. Figure 8.3 shows examples of such evolving IMFs. The two slope IMF with $M_{\text{break}} = 0.5 M_\odot$ and the Chabrier IMF with $M_c = 0.079 M_\odot$ (lines *a* and *c* in Figure 8.3) fit each other extremely well and both provide a good fit to the local empirical IMF. By moving the break/characteristic mass to higher values one can explore the effects of such evolving IMF, for example mimicking a systematic trend with redshift. The cases with $M_c \simeq M_{\text{break}} \simeq 4 M_\odot$ are

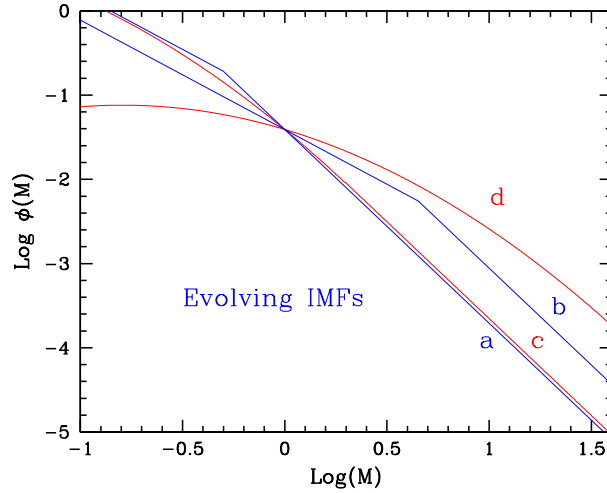


Figure 8.3: Examples of evolving IMFs, for a two-slope IMF and a Chabrier-like IMF. Lines *a* and *c* represent the local IMF. The other lines show modified IMFs to explore a hypothetical evolution with redshift, with the break mass and the characteristic mass M_c having increased to $\sim 4 M_\odot$, lines *b* and *d* respectively for the two-slope and the Chabrier-like IMF. All IMFs have been normalized to have the same value for $M = M_\odot$.

shown in Figure 8.3 (lines *b* and *d*). Having normalized all IMFs to the same

value of $\phi(M = 1 M_{\odot})$, Figure 8.3 allows one to immediately gauge the relative importance of massive stars compared to solar mass stars, with the latter ones providing the bulk of the light from old ($\gtrsim 10$ Gyr) populations.

8.2

The M/L Ratio of Elliptical Galaxies and the IMF Slope Below $1 M_{\odot}$

Figure 8.4 shows as a function of age the M_*/L_B ratio (where M_* is the stellar mass) for SSPs with solar composition, and different IMFs each with a single slope s over the whole mass range $0.1 \leq M \leq 100 M_{\odot}$. Very large mass-to-light ratios are produced by either very flat ($s = 1.35$) or very steep ($s = 3.35$) IMFs, whereas the Salpeter's slope gives the lowest values of the M_*/L_B ratio. This is a result of the different stellar demography already illustrated in Figures 8.1 and 8.2, such that a steep IMF is *dwarf dominated*, that is, most of the mass is in low-mass stars, whereas a flat IMF is *remnant dominated* and most of the mass is in dead remnants.

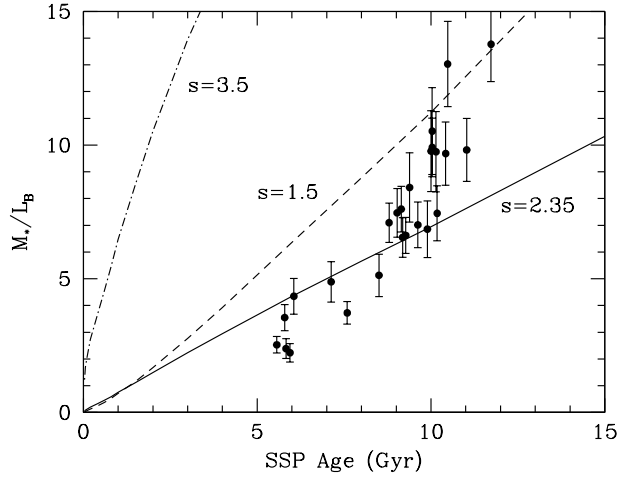


Figure 8.4: The stellar mass-to-light ratio of solar metallicity SSPs as a function of age, for three different single slope IMFs, from 0.1 to $100 M_{\odot}$. Also plotted are values of the dynamical M/L ratio for a sample of local elliptical galaxies with detailed dynamical modelling (source: M/L ratios for models: Maraston, C. (1998, *Mon. Not. R. Astron. Soc.*, 300, 872); for the data: Cappellari, M. *et al.* (2006, *Mon. Not. R. Astron. Soc.*, 366, 1126), van der Marel, R.P. and van Dokkum, P. (2007, *Astrophys. J.*, 668, 756), van Dokkum, P. and van der Marel, R.P. (2007, *Astrophys. J.*, 655, 30); ages: from Eq. (1) in Thomas, D. *et al.* (2010, *Mon. Not. R. Astron. Soc.*, 404, 1775)).

Measurements of the structure (e.g., half light radius) and stellar velocity dispersion of elliptical galaxies provide estimates of their *dynamical* mass, hence their dynamical mass-to-light ratio can be compared to the stellar M/L ratio. This is shown in Figure 8.4 for a sample of local elliptical galaxies with detailed dynamical modelling, having adopted a relation between the luminosity-

weighted age of their stellar populations and velocity dispersion, namely $\text{Log}(\text{Age}/\text{Gyr}) = -0.11 + 0.47 \text{Log}(\sigma_v)$, consistent with Eq. (6.16). Clearly very steep ($s = 3.5$) and very flat ($s = 1.5$) slopes of the IMF appear to be excluded by the data, whereas the intermediate (Salpeter) slope is quite consistent with the data, apart from the older galaxies which have a higher M/L ratio than the SSP models. However, besides an increase of age also the average metallicity is likely to increase with σ_v , with the galaxies in Figure 8.4 spanning a range from $\sim 1/2$ solar to ~ 2 times solar. Thus, the same galaxies are displayed again in Figure 8.5, together with model M/L ratios for a straight Salpeter IMF and three different metallicities. The trend in M/L ratio exhibited by the data appears to be consistent with the trend resulting from the metallicity trend with σ_v , and with a straight Salpeter IMF. However, things may not be as simple as they appear. Dark matter may contribute to the dynamical M/L ratios, and the IMF may not be straight Salpeter. A Salpeter-diet IMF such as that shown in Figure 8.1 would give M_*/L_B ratios systematically lower by $\sim 40\%$ than shown in these figures, thus opening some room for a dark matter contribution to the dynamical mass of these galaxies. Alternatively, an IMF slightly flatter than Salpeter at high masses, with its larger contribution by stellar remnants, would reproduce the high dynamical M/L ratios of the oldest galaxies, without dark matter contribution. It is quite difficult to circumvent this dark-matter/IMF degeneracy on the dynamical M/L ratios of elliptical galaxies.

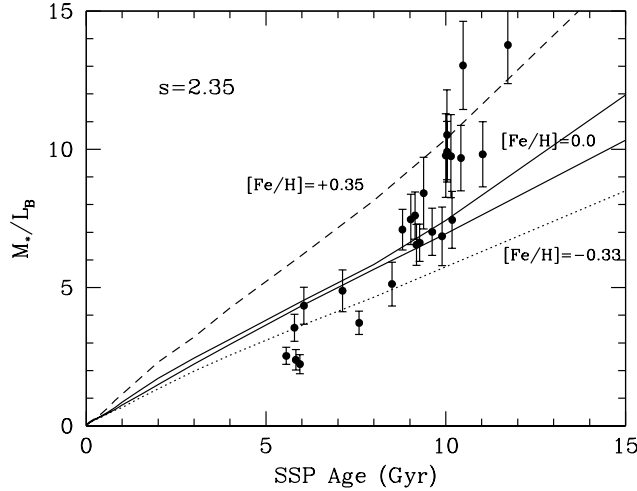


Figure 8.5: The M/L ratio of SSPs with a straight Salpeter IMF, for subsolar (dotted), supersolar (dashed) and solar metallicity (solid), as indicated. The two solid lines refer to two releases of the same set of SSP models (source: model M/L ratios are from Maraston, C. (1998, *Mon. Not. R. Astron. Soc.*, 300, 872; 2005, *Mon. Not. R. Astron. Soc.*, 362, 799); data points are the same as in Figure 8.4).

8.3

The Redshift Evolution of the M/L Ratio of Cluster Ellipticals and the IMF Slope Between ~ 1 and $\sim 1.4 M_\odot$

The slope of the IMF controls the rate of luminosity evolution of a SSP, as shown by Figure 2.6 for the bolometric light. The flatter the IMF the more rapid the luminosity declines past an event of star formation. On the contrary, the steeper the IMF the slower such decline, as the light from many low-mass stars compensates for the progressive death of the rarer, more massive and brighter stars. Having identified and studied passively evolving elliptical galaxies all the way to $z \sim 2$ and even beyond, one expects that their M/L ratio must systematically decrease with increasing redshift, and do so by an amount that depends on the slope of the IMF. This test is particularly effective if undertaken for cluster ellipticals, as clusters provide fairly numerous samples of ellipticals at well defined redshifts. Besides the IMF, the rate of luminosity (M/L) evolution also depends on the age of a SSP, being much faster at young ages than at late epochs. Thus, the rate of M/L evolution of elliptical galaxies with redshift must depend on both the IMF slope and the luminosity-weighted age of their stellar populations, or, equivalently on their formation redshift.

We know that the bulk of stars in local massive ellipticals are very old, and for an age of ~ 12 Gyr the light of such galaxies comes from a narrow range around the turnoff mass M_{TO} at $\sim 1 M_\odot$. Their progenitors at $z \sim 1.5$ must be younger by the corresponding lookback time, that is, ~ 9 Gyr younger, and from the M_{TO} –age relation (Eq. (2.2)) we see that the bulk of light of such progenitors has to come from stars of mass around $M_{\text{TO}} \simeq 1.4 M_\odot$. Thus, the evolution of the M/L ratio of old stellar populations from redshift zero all the way to redshift ~ 1.5 is controlled by the IMF slope in the narrow interval between ~ 1 and $\sim 1.4 M_\odot$. The IMF slope below $\sim 1 M_\odot$ has no influence on the luminosity evolution, and that above $\sim 1.4 M_\odot$ was in control of the luminosity evolution at redshifts beyond ~ 1.5 . Therefore, the evolution of the M/L ratio of elliptical galaxies from $z = 0$ to ~ 1 allows us to measure the slope of the IMF just near $M \sim 1 M_\odot$.

Figure 8.6 shows the evolution with redshift of the M_*/L_B ratio of solar composition SSPs, for various IMF slopes and different formation redshifts. Also plotted is the average M_*/L_B ratio of cluster ellipticals from the literature, from local clusters at $z \sim 0$ all the way to clusters at $z \sim 1.3$. A Salpeter slope ($s = 2.35$) fits the data for a formation redshift z_F between ~ 2 and ~ 3 , which is in pretty good agreement with both the formation redshift derived from age-dating local ellipticals in various ways, and with the observed rapid disappearance of quenched galaxies beyond $z \sim 2$. Assuming that the IMF at the formation redshift of ellipticals was like line *b* in Figure 8.3, then with $s = 1.3$ at $M = 1 M_\odot$ this IMF would require a formation redshift well beyond 3 in order to fit the data. Line *d* instead, with $s = 0.8$ at $M = 1 M_\odot$ would fail to match the data even assuming $z_F = \infty$, as shown in Figure 8.6. One can conclude that the evolution of the M/L ratio of cluster elliptical galaxies up to redshift ~ 1.3 does not favor any significant departure from the Salpeter value $s = 2.35$ of the slope of the IMF in the vicinity of $M \sim 1 M_\odot$, all the way to a formation redshift beyond ~ 2 .

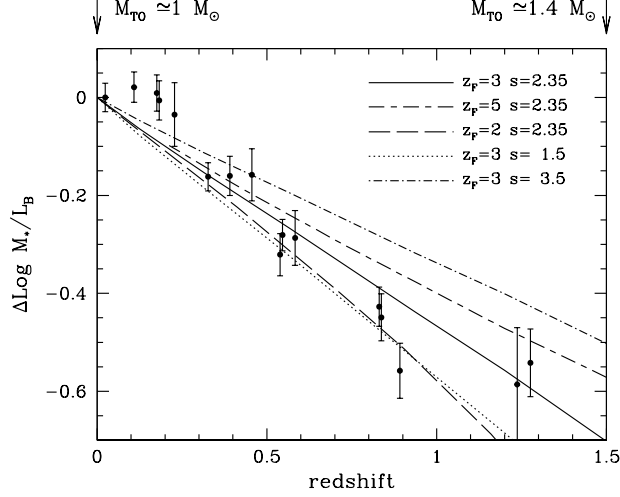


Figure 8.6: The differential redshift evolution (with respect to the value at $z = 0$) of the M_*/L_B mass-to-light ratio of solar composition SSPs, for various choices of the IMF slope between ~ 1 and $\sim 1.4 M_\odot$, and for various assumed formation redshifts z_F , as indicated. The data points refer to the M_*/L_B ratio of elliptical galaxies in clusters at various redshifts, from $z \sim 0$ up to $z \simeq 1.3$. (Updated from Renzini, A. (2005) *The Initial Mass Function 50 Years later*, (ed. E. Corbelli *et al.*, *Ap. Sp. Sci. Library*, 327, 221.).

8.4

The Metal Content of Galaxy Clusters and the IMF Slope Between ~ 1 and $\sim 40 M_\odot$, and Above

In its youth, a stellar population generates lots of UV photons, core collapse supernovae and metals that go to enrich the ISM. In its old age, say ~ 12 Gyr later, the same stellar population radiates optical-near-IR light from its $\sim 1 M_\odot$ stars, while all more massive stars are dead remnants. The amount of metals (M_X) that are produced by such populations is proportional to the number of massive stars $M \gtrsim 8 M_\odot$ that have undergone a core collapse supernova explosion, whereas the luminosity (e.g., L_B) at $t \simeq 12$ Gyr is proportional to the number of stars with $M \sim 1 M_\odot$. It follows that the metal-mass-to-light ratio M_X/L_B is a measure of the number ratio of massive to $\sim M_\odot$ stars, that is, of the IMF slope between ~ 1 and $\sim 40 M_\odot$. Clusters of galaxies offer an excellent opportunity to measure both the light of their dominant stellar populations, and the amount of metals that such populations have produced in their early days. Indeed, most of the light of clusters of galaxies comes from ~ 12 Gyr old, massive ellipticals, and the abundance of metals can be measured both in their stellar populations and in the intracluster medium (ICM). Iron is the element whose abundance can be most reliably measured both in cluster galaxies and in the ICM, but its production is likely to be dominated by Type Ia supernovae whose progenitors are binary stars. As extensively discussed in Chapter 7, a

large fraction of the total iron production comes from Type Ia supernovae, and the contribution from CC supernovae is uncertain; therefore the $M_{\text{Fe}}/L_{\text{B}}$ ratio of clusters is less useful to set constraints on the IMF slope between ~ 1 and $M \gtrsim 10 M_{\odot}$. For this reason, we focus on oxygen and silicon, whose production is indeed dominated by core collapse supernovae.

Following the notations in Chapter 2, the IMF can be written as:

$$\phi(M) = a(t, Z) L_{\text{B}} M^{-s}, \quad (8.4)$$

where $a(t, Z)$ is the relatively slow function of SSP age and metallicity shown in Figure 2.10, multiplied by the bolometric correction shown in Figure 3.1. Thus, the metal-mass-to-light ratio for the generic element “X” can be readily calculated from:

$$\frac{M_{\text{X}}}{L_{\text{B}}} = \frac{1}{L_{\text{B}}} \int_8^{120} m_{\text{X}}(M) \phi(M) dM = a(t, Z) \int_8^{120} m_{\text{X}}(M) M^{-s} dM, \quad (8.5)$$

where $m_{\text{X}}(M)$ is the mass of the element X which is produced and ejected by a star of mass M . From stellar population models one has $a(12 \text{ Gyr}, Z) = 2.22$ and 3.12 , respectively, for $Z = Z_{\odot}$ and $2Z_{\odot}$ and we adopt $a(12 \text{ Gyr}) = 2.5$ in Eq. (8.5). Using the oxygen and silicon yields $m_{\text{O}}(M)$ and $m_{\text{Si}}(M)$ from theoretical nucleosynthesis (cf. Figure 7.5), Equation (8.5) then gives the $M_{\text{O}}/L_{\text{B}}$ and $M_{\text{Si}}/L_{\text{B}}$ metal mass-to-light ratios that are reported in Figure 8.7 as a function of the IMF slope between ~ 1 and $\sim 40 M_{\odot}$. As expected, the $M_{\text{O}}/L_{\text{B}}$ and $M_{\text{Si}}/L_{\text{B}}$ are extremely sensitive to the IMF slope. The values observed in local clusters of galaxies, from X-ray observations of the ICM and assuming stars are near solar on average, are ~ 0.1 and $\sim 0.008 M_{\odot}/L_{\odot}$, respectively for oxygen and silicon, as documented in Chapter 10. These empirical values are also displayed in Figure 8.7. A comparison with the calculated values shows that with the Salpeter IMF slope ($s = 2.35$) the standard explosive nucleosynthesis from core collapse supernovae produces just the right amount of oxygen and silicon to match the observed $M_{\text{O}}/L_{\text{B}}$ and $M_{\text{Si}}/L_{\text{B}}$ ratios in clusters of galaxies, having assumed that most of the B -band light of clusters comes from ~ 12 Gyr old populations. Actually, silicon may be even somewhat overproduced if one allows a $\sim 40\%$ contribution from Type Ia supernovae (cf. Figure 7.17).

Figure 8.7 also shows that with $s = 1.35$ such a top heavy IMF would overproduce oxygen and silicon by more than a factor ~ 20 . Such a huge variation with $\Delta s = 1$ is actually expected, given that for a near Salpeter slope the typical mass of metal producing stars is $\sim 25 M_{\odot}$. By the same token, the IMF labelled b in Figure 8.3 would overproduce metals by a factor ~ 4 with respect to a Salpeter-slope IMF (lines a and c), whereas the IMF labelled d in Figure 8.3 would do so by a factor ~ 20 . Thus, under the assumptions that the bulk of the light of local galaxy clusters comes from ~ 12 Gyr old stars, that current stellar theoretical nucleosynthesis is basically correct, and that no large systematic errors affect the reported empirical values of the $M_{\text{O}}/L_{\text{B}}$ and $M_{\text{Si}}/L_{\text{B}}$ ratios, then one can exclude a significant evolution of the IMF with cosmic time, such as for example, one in which the IMF at $z \sim 3$ would be represented by line b or d in Figure 8.3, and by line a or c at $z = 0$.

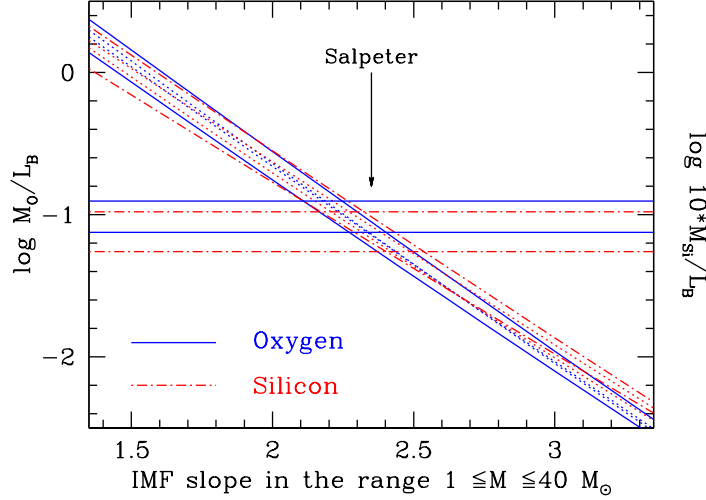


Figure 8.7: The oxygen and silicon mass-to-light ratios as a function of the IMF slope for a ~ 12 Gyr old, near solar metallicity SSP with oxygen and silicon yields from standard nucleosynthesis calculations. Different lines refer to the different theoretical yields shown in Figure 7.5a,b. The horizontal lines show the uncertainty range of the observed values of these ratios in clusters of galaxies, with central values as reported in Chapter 10, and allowing for a $\sim \pm 25\%$ uncertainty.

— OOO —

A variable IMF is often invoked as an *ad hoc* fix to specific discrepancies that may emerge here or there, which however may have other origins. For example, an evolving IMF with redshift has been sometimes invoked to ease a perceived discrepancy between the cosmic evolution of the stellar mass density, and the integral over cosmic time of the star formation rate. In other contexts it has been proposed that the IMF may be different in starbursts as opposed to more steady star formation, or in disks vs. spheroids. Sometimes one appeals to a top-heavy IMF in one context, and then to a bottom-heavy one in another, as if it was possible to have as many IMFs as problems to solve. Honestly, we do not know whether there is one and only one IMF. However, if one subscribes to a different IMF to solve a single problem, then at the same time one should make sure the new IMF does not destroy agreements elsewhere, or conflicts with other astrophysical constraints. While it is perfectly legitimate to contemplate IMF variations from one situation to another, it should be mandatory to explore all consequences of postulated variations, well beyond the specific case one is attempting to fix. This kind of sanitary check is most frequently neglected in the literature appealing to IMF variations. A few examples of such checks have been presented in this chapter.

Further readings

This chapter expands and updates the paper: Renzini, A. (2005) *The Initial Mass Function 50 Years later*, ed. E. Corbelli *et al.* , Ap. Sp. Sci. Library, 327, 221.

Most Popular Initial Mass Functions

Chabrier, G. (2003) *Publ. Astron. Soc. Pac.*, **115**, 763.

Kroupa, P. (2002) *Science*, **295**, 82.

Salpeter, E.E. (1955) *Astrophys. J.*, **121**, 161.

Scalo, J.M. (1986) *Fund. Cosm. Phys.*, **11**, 1.

Recent review

Bastian, N. et al. (2010) *Annu. Rev. Astron. Astrophys.*, **48**, 339.

The IMF at High Redshift

Davé, R. (2008) *Mon. Not. R. Astron. Soc.*, **385**, 147.

Tacconi, L.J. (2008) *Astrophys. J.*, **680**, 246.

van Dokkum, P. G. (2008) *Astrophys. J.*, **674**, 29.

Table of Contents of the whole book

1 Firm and Less Firm Outcomes of Stellar Evolution Theory	1
1.1 A Brief Journey through Stellar Evolution	1
1.1.1 A $9 M_{\odot}$ Star	1
1.1.2 The Evolution of Stars with Solar Composition	8
1.1.3 Dependence on Initial Chemical Composition	12
1.1.4 The Asymptotic Giant Branch Phase	15
1.2 Strengths and Weaknesses of Stellar Evolutionary Models	18
1.2.1 Microphysics	19
1.2.2 Macrophysics	20
1.3 The Initial Mass-Final Mass Relation	31
 2 The Fundamentals of Evolutionary Population Synthesis	 35
2.1 The Stellar Evolution Clock	35
2.2 The Evolutionary Flux	38
2.3 The Fuel Consumption Theorem	39
2.4 Fuel Consumptions	42
2.5 Population Synthesis Using Isochrones	46
2.6 The Luminosity Evolution of Stellar Populations	47
2.7 The Specific Evolutionary Flux	49
2.8 The IMF Scale Factor	51
2.9 Total and Specific Rates of Mass Return	52
2.10 Mass and Mass-to-Light Ratio	56
2.11 IMF-Dependent and IMF-Independent Quantities	57
2.12 The Age-Metallicity Degeneracy	58
 3 Resolving Stellar Populations	 61
3.1 The Stellar Populations of Pixels and Frames	61
3.1.1 The Stellar 1 Population of a Frame	61
3.1.2 The Stellar Population of a Pixel	64
3.2 Simulated Observations and Their Reduction	68
 4 Age Dating Resolved Stellar Populations	 77
4.1 Globular Cluster Ages	77
4.1.1 Absolute and Relative Globular Cluster Ages	78
4.1.2 Globular Clusters with Multiple Populations	80
4.2 The Age of the Galactic Bulge	83
4.3 Globular Clusters in the Magellanic Clouds	86
4.4 Stellar Ages of the M31 Spheroid	88
4.4.1 The Bulge of M31	88
4.4.2 The M31 Halo and Giant Stream	90
4.5 The Star Formation Histories of Resolved Galaxies	92
4.5.1 The Mass-Specific Production	93
4.5.2 Decoding the CMD	98

4.5.3 The Specific Production Method	102
4.5.4 The Synthetic CMD Method	104
4.5.5 An Example: the Stellar Population in the Halo of the Centaurus A Galaxy	106
5 The Evolutionary Synthesis of Stellar Populations	113
5.1 Simple Stellar Populations	113
5.2 Spectral Libraries	115
5.2.1 Empirical Spectral Libraries	115
5.2.2 Model Atmosphere Libraries	116
5.3 Composite Stellar Populations	116
5.4 Evolving Spectra	118
5.4.1 The Spectral Evolution of a SSP	118
5.4.2 The Spectral Evolution of Composite Stellar Populations	121
5.4.3 There are Also Binaries	128
6 Stellar Population Diagnostics of Galaxies	133
6.1 Measuring Star Formation Rates	133
6.1.1 The SFR from the Ultraviolet Continuum	134
6.1.2 The SFR from the Far-Infrared Luminosity	136
6.1.3 The SFR from Optical Emission Lines	137
6.1.4 The SFR from the Soft X-ray Luminosity	138
6.1.5 The SFR from the Radio Luminosity	139
6.2 Measuring the Stellar Mass of Galaxies	140
6.3 Age and Metallicity Diagnostics	143
6.3.1 Star-Forming Galaxies	143
6.3.2 Quenched Galaxies	145
6.4 Star-Forming and Quenched Galaxies through Cosmic Times	153
6.4.1 The Main Sequence of Star-Forming Galaxies	155
6.4.2 The Mass and Environment of Quenched Galaxies	163
6.4.3 Mass Functions	164
7 Supernovae	171
7.1 Observed SN Rates	173
7.2 Core Collapse SNe	175
7.2.1 Theoretical Rates	176
7.2.2 Nucleosynthetic Yields	179
7.3 Thermonuclear Supernovae	184
7.3.1 Evolutionary Scenarios for SNIa Progenitors	185
7.3.2 The Distribution of Delay Times	187
7.3.3 The SD Channel	188
7.3.4 The DD Channel	191
7.3.5 Constraining the DTD and the SNIa Productivity	197
7.3.6 SNIa Yields	201

8 The IMF From low to High Redshift	207
8.1 How the IMF Affects Stellar Demography	208
8.2 The M/L Ratio of Elliptical Galaxies and the IMF Slope Below $1 M_{\odot}$	211
8.3 The Redshift Evolution of the M/L Ratio of Cluster Ellipticals and the IMF Slope Between ~ 1 and $\sim 1.4 M_{\odot}$	213
8.4 The Metal Content of Galaxy Clusters and the IMF Slope Between ~ 1 and $\sim 40 M_{\odot}$, and Above	214
 9 Evolutionary Links Across Cosmic Time: an Empirical History of Galaxies	219
9.1 The Growth and Overgrowth of Galaxies	221
9.2 A Phenomenological Model of Galaxy Evolution	224
9.2.1 How Mass Quenching Operates	225
9.2.2 How Environmental Quenching Operates	227
9.2.3 The Evolving Demography of Galaxies	229
9.2.4 Caveats	232
9.2.5 The Physics of Quenching	234
 10 The Chemical Evolution of Galaxies, Clusters, and the Whole Universe	237
10.1 Clusters of Galaxies	237
10.1.1 Iron in the Intracluster Medium and the Iron Mass-to-Light Ratio	238
10.1.2 The Iron Share Between ICM and Cluster Galaxies	244
10.1.3 Elemental Ratios	245
10.1.4 Metal Production: the Parent 1 Stellar Populations	247
10.1.5 Iron from SNIa	248
10.1.6 Iron and Metals from Core Collapse SNe	249
10.2 Metals from Galaxies to the ICM: Ejection versus Extraction	250
10.3 Clusters versus Field and the Overall Metallicity of the Universe	252
10.4 Clusters versus the Chemical Evolution of the Milky Way	254